The EMBO Journal (2010) 29, 843–854 | © 2010 European Molecular Biology Organization | All Rights Reserved 0261-4189/10
www.embojournal.org

THE EMBO JOURNAL

Kinesin-1/Hsc70-dependent mechanism of slow axonal transport and its relation to fast axonal transport

Sumio Terada[1,2,3], Masataka Kinjo[4], Makoto Aihara[5], Yosuke Takei[1] and Nobutaka Hirokawa[1,*]

[1]Department of Cell Biology and Anatomy, University of Tokyo Graduate School of Medicine, Bunkyo-ku, Tokyo, Japan, [2]Section of Neuroanatomy and Cellular Neurobiology, Department of Systems Neuroscience, Centre for Brain Integration Research, Tokyo Medical and Dental University Graduate School of Medical and Dental Sciences, Bunkyo-ku Tokyo, Japan, [3]PRESTO: Precursory Research for Embryonic Science and Technology, Japan Science and Technology Agency, Kawaguchi, Saitama, Japan, [4]Laboratory of Molecular Cell Dynamics, Faculty of Advanced Life Science, Hokkaido University, Sapporo, Hokkaido, Japan and [5]Department of Ophthalmology, University of Tokyo Graduate School of Medicine, Bunkyo-ku, Tokyo, Japan

Cytoplasmic protein transport in axons ('slow axonal transport') is essential for neuronal homeostasis, and involves Kinesin-1, the same motor for membranous organelle transport ('fast axonal transport'). However, both molecular mechanisms of slow axonal transport and difference in usage of Kinesin-1 between slow and fast axonal transport have been elusive. Here, we show that slow axonal transport depends on the interaction between the DnaJ-like domain of the kinesin light chain in the Kinesin-1 motor complex and Hsc70, scaffolding between cytoplasmic proteins and Kinesin-1. The domain is within the tetratricopeptide repeat, which can bind to membranous organelles, and competitive perturbation of the domain in squid giant axons disrupted cytoplasmic protein transport and reinforced membranous organelle transport, indicating that this domain might have a function as a switchover system between slow and fast transport by Hsc70. Transgenic mice overexpressing a dominant-negative form of the domain showed delayed slow transport, accelerated fast transport and optic axonopathy. These findings provide a basis for the regulatory mechanism of intracellular transport and its intriguing implication in neuronal dysfunction.

The EMBO Journal (2010) **29,** 843–854. doi:10.1038/emboj.2009.389; Published online 28 January 2010
Subject Categories: membranes & transport; neuroscience
Keywords: axonal transport; chaperone; Hsc70; kinesin light chain; tetratricopeptide repeat

*Corresponding author. Department of Cell Biology and Anatomy, University of Tokyo Graduate School of Medicine, 7-3-1 Hongo, Bunkyo-ku, Tokyo 113-0033, Japan. Tel.: +81 3 5841 3326; Fax: +81 3 5802 8646; E-mail: hirokawa@m.u-tokyo.ac.jp

Received: 2 September 2009; accepted: 26 November 2009; published online: 28 January 2010

Introduction

Neurons develop long axons and dendrites to convey information. This morphology requires neurons to possess a highly developed transport system (Grafstein and Forman, 1980; Hirokawa and Noda, 2008). After synthesis in the cell body, proteins are transported down the axon as various kinds of membrane organelles or protein complexes. Through observation of transected axons (Wallerian degeneration), nerve ligation experiments and metabolic radiolabelling studies, fast and slow axonal transport systems have been defined. In contrast to the discovery of Kinesin-1 and the kinesin superfamily as fast transport motors mainly for membranous organelles (Hirokawa and Takemura, 2005; Hirokawa and Noda, 2008), the molecular mechanism of slow transport for cytoplasmic proteins has been enigmatic (Baas and Brown, 1997; Hirokawa *et al*, 1997; Nixon, 1998; Galbraith and Gallant, 2000; Brown, 2003; Terada, 2003).

Earlier, we found that labelled tubulin and other cytosolic proteins injected into squid giant axons were transported in a Kinesin-1-dependent manner (Terada *et al*, 2000). To create a unified view of the Kinesin-1-based transport system for both cytosolic and membranous proteins, we need to scrutinize the nature of the transporting complex. Considering the limited numbers of molecular motors disclosed by the genome project and the large number of transported proteins, each motor must be responsible for transport of multiple protein cargoes.

We noted that chaperone molecules were promising candidates for linking the Kinesin-1 complex to cytoplasmic proteins. The chaperones can interact with various cytoplasmic proteins non-specifically, and the possible concurrent control mechanism of cargo protein activity and its transport by them was an attractive hypothesis. Among these, Hsc70 drew our attention, as it is transported at a slow rate in axons (de Waegh and Brady, 1989; Bourke *et al*, 2002), can interact with various motor complex proteins including Kinesin-1 and binds to the kinesin light chain (KLC) through the DnaJ-like domain within the tetratricopeptide repeat (TPR) of KLC (Tsai *et al*, 2000).

We evaluated this hypothesis using immunoprecipitation and real-time observation system of slow axonal transport in squid giant axons (Terasaki *et al*, 1995; Galbraith *et al*, 1999; Terada *et al*, 2000), and analysed the putative transporting complex of slow axonal transport by fluorescence cross-correlation spectroscopy (FCCS) (Rigler and Elson, 2001; Kim and Schwille, 2003; Saito *et al*, 2004). Through these experiments, we discovered an unexpected putative switchover system between slow and fast axonal transport by Hsc70, through the DnaJ-like domain of KLC, and generated transgenic mice with retarded slow and accelerated fast axonal transport by modifying the interaction between the Kinesin-1 complex and Hsc70. Superficially, these mice appeared to be healthy, except for a slight modification in

axonal transport. Towards the end of their life span, however, they showed slowly progressive optic nerve axonopathy. On the basis of our results, we discuss a new model of intracellular transport regulation and its likely relevance to neuronal dysfunction and disorders.

Results

KLC/Hsc70/creatine kinase are immunoprecipitated as a complex and their association is regulated by DnaJ-like domain and ATP

To show the interaction among the possible complex of KLC/Hsc70/creatine kinase (cytosolic protein), we performed immunoprecipitation, using mouse sciatic nerve axons (Figure 1). Each of anti-KLC, Hsc70 and creatine kinase antibodies co-immunoprecipitated with the other two of the complex (Figure 1A–C) and the interaction between KLC and Hsc70 is reduced when the KLC DnaJ-like domain peptide fragment (J-domain, 5 mM) was added in the solution in the presence of ATP (2 mM) (Figure 1A and B). When ATP is depleted by apyrase treatment, the DnaJ-like domain peptide effect on creatine kinase dissociation from the Hsc70 was reduced, suggesting that the ADP form of Hsc70, that is DnaJ domain protein-binding form, could carry the cytosolic protein cargoes more effectively (Figure 1B and C).

DnaJ-like domain peptide of KLC inhibits creatine kinase transport in squid giant axons

Next, we injected Alexa 488-labelled creatine kinase, a typical component of slow axonal transport (Brady and Lasek, 1981; Terada *et al*, 2000), into squid giant axons, and monitored the anterograde movement of the fluorescent transport profile along the longitudinal axis of the axon by confocal laser scanning microscopy (CLSM) (Terasaki *et al*, 1995; Terada *et al*, 1996, 2000; Galbraith *et al*, 1999) (Figure 2A). We chose creatine kinase as a marker for slow axonal transport, because various cytoplasmic proteins including creatine kinase are transported in squid giant axons (Terada *et al*, 2000). Their transport was dependent on microtubules, and inhibited by AMP-PNP reversibly. In extruded axoplasm, anti-Kinesin-1 antibody blocked their transport. In the case for creatine kinase, functional blocking antibody (Fab fragment) against Kinesin-1 (H2, 0.4 mg/ml) suppressed the movement during the first 20 min from injection (P-value $0.00 < 0.05$, Mann–Whitney test). Control normal mouse IgG Fab fragment did not block the transport and depletion of H2 Fab fragment by recombinant Kinesin-1 beads cancelled the inhibition by this antibody. Electron microscopic examination ruled out the possible specific structural damage by antibody treatment (data not shown). On the basis of these data, we confirmed that creatine kinase transport in squid giant axons is dependent on Kinesin-1.

To examine the relevance of the DnaJ-like domain of KLC as a scaffold for cytoplasmic protein transport through Hsc70 binding, we co-injected a KLC DnaJ-like domain peptide fragment (5 mM) with creatine kinase and followed the movement profile (Figure 2B). Compared with no peptide or control peptides with the reverse sequence of a KLC DnaJ-like domain (Figure 2C), and two other reverse sequences of the carboxy terminal of Hsc70, creatine kinase transport was inhibited, especially in the early phase (<30 min) after injection (Figure 2D; all P-values <0.05, Mann–Whitney tests). After giving time for the peptide to diffuse away, the transport regained its normal profile, indicating that this inhibitory effect was reversible (Figure 2B; late phase (30–70 min after the injection)). From our data, the transport regains after 30 min from injection, thus we consider that the local concentration of the peptide decreases under the effective concentration in half an hour. We could consistently observe the transport recovery during 30–60 min after injection. Earlier electrophysiological experiments using squid neurons indicate that microinjected functional peptides (0.1–1 pl of 2–20 mM solution) of the similar size show effects immediately after injection for about 30 min (Hilfiker *et al*, 2005; Moreno *et al*, 2009). Regarding the time course of peptide effect because of diffusion in the squid cytoplasm, our experimental results are well comparable with these findings. We experienced dose-dependent inhibitory effect (from 1 to 10 mM solution) by the DnaJ-like domain peptide, especially in the early phase, and in our case, 5 mM solution was sufficient to cause the constant effect in different series of experiments (data not shown).

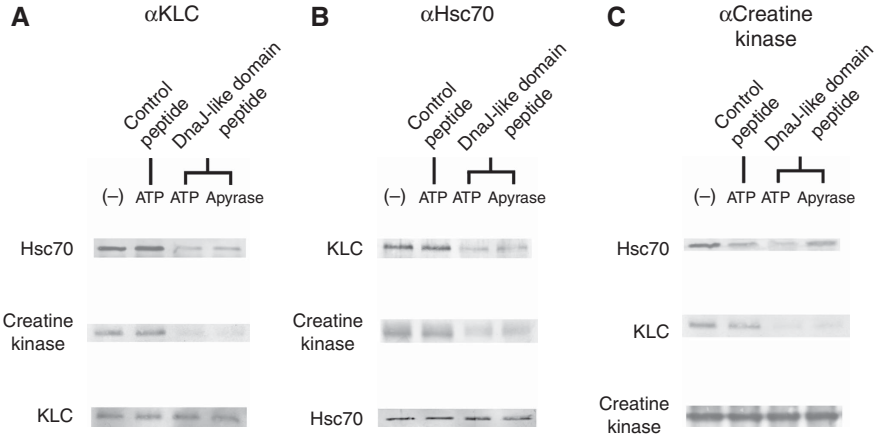

Figure 1 Co-immunoprecipitation of KLC/Hsc70/creatine kinase complex in sciatic nerve preparation. Co-immunoprecipitation results using anti-KLC (**A**), Hsc70 (**B**) and creatine kinase (**C**) antibodies are shown, combined with experimental conditions on KLC DnaJ-like domain peptide fragment of KLC, ATP, apyrase or reversed DnaJ-like domain control peptide addition.

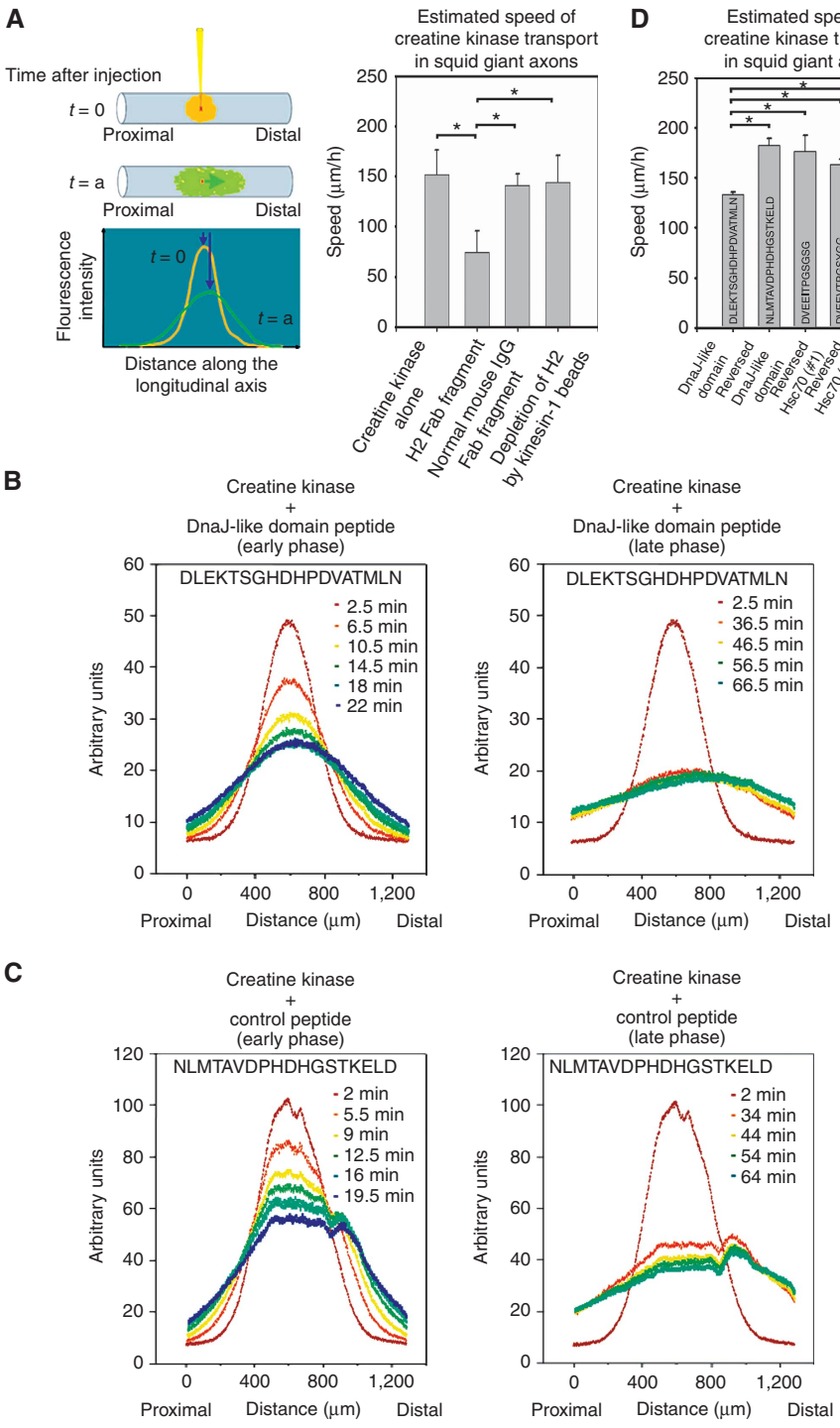

Figure 2 DnaJ-like domain peptide of KLC and the creatine kinase transport in squid giant axons. (**A**) Injection of labelled creatine kinase into squid giant axons and monitoring of the profile movement. The movement is blocked by anti-Kinesin-1 antibody. After injection ($t=0$), the fluorescent signal profile was measured time sequentially ($t=$a) along the longitudinal axis of the axon. Each profile was fitted with Gaussian curve, and the transporting speed of its gravity centre was estimated. The transporting profile moved anterogradely (note that the right direction is distal). Anti-Kinesin-1 antibody inhibits creatine kinase transport in the early phase. Each bar shows standard deviation. Estimated average speeds ± standard deviation: creatine kinase alone, 151.3 ± 24.4 μm/h ($n=4$); functional blocking antibody (Fab fragment) against Kinesin-1 (H2, 0.4 mg/ml), 74.2 ± 21.1 μm/h ($n=4$); control normal mouse IgG Fab fragment, 140.5 ± 11.5 μm/h ($n=4$); depletion of H2 Fab fragment by recombinant Kinesin-1 beads, 143.7 ± 26.6 μm/h ($n=4$). All *P*-values of the pairs with asterisks are $0.00<0.05$, Mann–Whitney tests. (**B**, **C**) Co-injection of a DnaJ-like domain peptide (**B**) or control peptide (**C**) with creatine kinase and monitoring of the profile movements. The early phases (<30 min) after the injection are on the left, whereas the late phases (30–70 min) are on the right. (**D**) DnaJ-like domain peptide inhibits creatine kinase transport in the early phase. Each bar shows standard deviation. Estimated average speeds ± standard deviation: DnaJ-like domain peptide, 133.1 ± 2.3 μm/h ($n=4$); reversed sequence of DnaJ-like domain peptide fragment, 182.4 ± 7.0 μm/h ($n=5$); reversed sequence of the carboxy terminal of Hsc70 (#1), 176.1 ± 16.0 μm/h ($n=4$); reversed sequence of the carboxy terminal of Hsc70 (#2), 163.2 ± 5.0 μm/h ($n=4$); creatine kinase alone without peptides, 179.2 ± 6.2 μm/h ($n=4$), $P=0.032$ (DnaJ-like domain peptide and reversed DnaJ-like domain peptide); 0.029 (DnaJ-like domain peptide and reversed Hsc70 #1 peptide), 0.029 (DnaJ-like domain peptide and reversed Hsc70 #2 peptide); 0.032 (DnaJ-like domain peptide and creatine kinase alone). All *P*-values <0.05, Mann–Whitney tests. Peptide sequence used in each case is indicated in the bar.

DnaJ-like domain peptide disrupts formation of the transporting complex

Next, we used FCCS to evaluate the effect of the DnaJ-like domain peptide on slow axonal transport. FCCS quantitatively measures the extent to which different fluorescent substances, Alexa 488-creatine kinase and Cy5-Hsc70 in the present case, coordinately redistribute in space as a function of time. The model data illustrated in Figure 3A show the following well established principles of FCCS (Rigler and Elson, 2001; Kim and Schwille, 2003; Saito *et al*, 2004). Large amplitude oscillation of cross-correlation within short-time ranges represents artifactual electrical noise and can be ignored. Correlation signals ($G(\tau)$) arise when the signal fluctuations from different molecules are statistically correlated, and indicate that the fluorescent substances interact directly or indirectly. Substantial interaction is indicated by cross-correlation signals that begin at values at least slightly higher than 1.0 and then gradually decay over time to base line ($G(\tau) = 1$). In contrast, cross-correlation signals that begin at base line and do not decay with time indicate little or no interaction. Actual correlation values oscillate around best-fit lines calculated as described in Materials and methods.

Using the squid giant axon paradigm described in Figure 2A, we performed FCCS measurements. Three representative sets of correlation curves from three different axons (out of >50 experiments for each condition) in Figure 3B (upper, middle and lower columns) indicate examples of simultaneous time-series measurement of Hsc70/creatinine kinase autocorrelations and their cross-correlation. We detected cross-correlation between microinjected Cy5-Hsc70 and Alexa 488-creatine kinase in both the absence and presence of a co-injected, control peptide (Figure 3B, upper right and middle right panels). The clear decay curves of cross-correlation in these cases indicated significant interactions between the Hsc70 and creatine kinase. In contrast, when we co-injected the DnaJ-like domain peptide with the fluorescent proteins, the amplitude of cross-correlation oscillated around base line and no signal decay was evident (Figure 3B, lower right panel). Together with the earlier results, these findings imply that the DnaJ-like domain peptide inhibited slow axonal transport by disrupting the transporting complex consisting of Kinesin-1 (KHC/KLC), Hsc70 and creatine kinase (Figure 3C).

In both the presence and absence of the DnaJ-like domain peptide, the autocorrelation curves of Hsc70 (Figure 3B, left panels) were fit best by a two-component model. This implies that the fluctuation of fluorescent signal from Hsc70 within the observation volume was due to a combination of small/readily movable and larger/less movable molecular complexes. Regardless of whether or not the DnaJ-like domain peptide was present, $\sim 65 \pm 10\%$ of the signal was due to the small/readily movable complexes, with the remainder being larger/less movable. The DnaJ domain peptide did have a major effect, however, on the average time for larger/less movable Hsc70 to diffuse through the observation volume, suggesting that this component could be involved in transport mechanism. The average diffusion time in the presence of the control peptide was $3900 \pm 2200\,\mu s$, but rose to $7300 \pm 6800\,\mu s$ when the DnaJ domain peptide was present. In contrast, the DnaJ domain peptide had little, if any effect on diffusion of small/readily movable Hsc70. The times required for this component to diffuse through the observation volume in the presence of the control peptide or the DnaJ domain peptide were 410 ± 130 or $510 \pm 210\,\mu s$, respectively.

In contrast to Hsc70, the autocorrelation curves for creatine kinase (Figure 3B, middle panels) were fit best by a one-component model of small/readily movable molecules. The average times for creatine kinase to diffuse through the observation volume were 610 ± 250 or $640 \pm 1200\,\mu s$ in the presence of the control or DnaJ domain peptide, respectively. As autocorrelation curve fitting evaluate diffusion behaviour of labelled biomolecules collectively and estimate rough grouping of molecular behaviour, very small amount of specific molecular populations might be overlooked. The facts that autocorrelation curves for creatine kinase are both best fit by one-component model, and their estimated diffusion time was not different indicate that single fluorescence correlation spectroscopy cannot detect the small population of molecules on slow axonal transport. Only FCCS measurement successfully detected the small population of Hsc70 and creatine kinase complex during slow axonal transport. (From these consequences, we consider that autocorrelation curves for Hsc70 best fit by two-component model do not detect the small population of Hsc70 and creatine kinase complex, either.) When considered collectively, the autocorrelation data for Hsc70 and creatine kinase suggest that Hsc70 is mainly present in the cytoplasm in two forms, monomeric and complex (Kim *et al*, 1992; Benaroudj *et al*, 1995), and that a very small fraction of creatine kinase is associated with the complexed form of Hsc70.

The cross-correlation curves between microinjected Cy5-Hsc70 and Alexa 488-creatine kinase in the presence of the co-injected, control peptide were fitted by a one-component

Figure 3 FCCS analysis of the creatine kinase transporting complex in squid giant axons. (**A**) (Left) Block diagram of the FCCS setup. Injected axons are excited with laser beams, and emission light is detected by an avalanche photodiode (APD). Fluctuations in the fluorescent signals are analysed using a digital correlator system. DM, dichroic mirror. (Middle) Schematic diagram of the FCCS measuring volume. The circular marks (green and red) represent Brownian movement of the fluorescent molecules. The movements of associated green and red marks are shown in grey. (Right) Schematic time trace of the fluorescence fluctuation (upper), calculated autocorrelation function (middle) and cross-correlation (lower) of fluorescent molecules in the measuring volume. Fitting lines with theoretical equations are indicated as smooth lines. (**B**) Three representative sets of correlation curves from three different axons (upper, middle and lower columns), indicating examples of simultaneous time-series measurement of Hsc70/creatinine kinase autocorrelations and their cross-correlation. Measured correlation curves in axons in peptide-free (upper), control peptide-containing (middle) and DnaJ-like domain peptide-containing (lower) conditions. The left, middle and right panels show the results for Hsc70, creatine kinase and the cross-correlation, respectively. (**C**) Direct relevance to the slow axonal transport system and deduced function of the Hsc70-KLC interaction. (Left) Scaffolding function of Hsc70 between KLC and creatine kinase. (Right) A peptide fragment of the DnaJ-like domain of KLC (red small triangle) disrupts creatine kinase transport by disrupting the cargo and motor interaction. The peptide competes the association between Hsc70 and KLC, thus disrupting the interaction between them. Dissociated Hsc70 is converted into the ATP form, thus releasing cytosolic protein(s). KHC: kinesin heavy chain (Kinesin-1).

model (47 samples out of 56 fitting trials), and the estimated diffusion time of successfully fitted samples was 470 ± 220 μs, suggesting that in majority of the samples, cross-correlation signal reflecting Hsc70 and creatine kinase complex does exist. On the other hand, in the case of the co-injected DnaJ-like domain peptide, only 6 samples out of 84 trials were fitted by a one-component model, suggesting that in majority of the samples, cross-correlation signal disappeared. Success rate for data fitting to the cross-correlation curves was higher when the co-injected, control peptide was present than when the DnaJ-like domain peptide was co-injected instead ($P = 0.000 < 0.001$, χ^2 test). Thus, the DnaJ-like

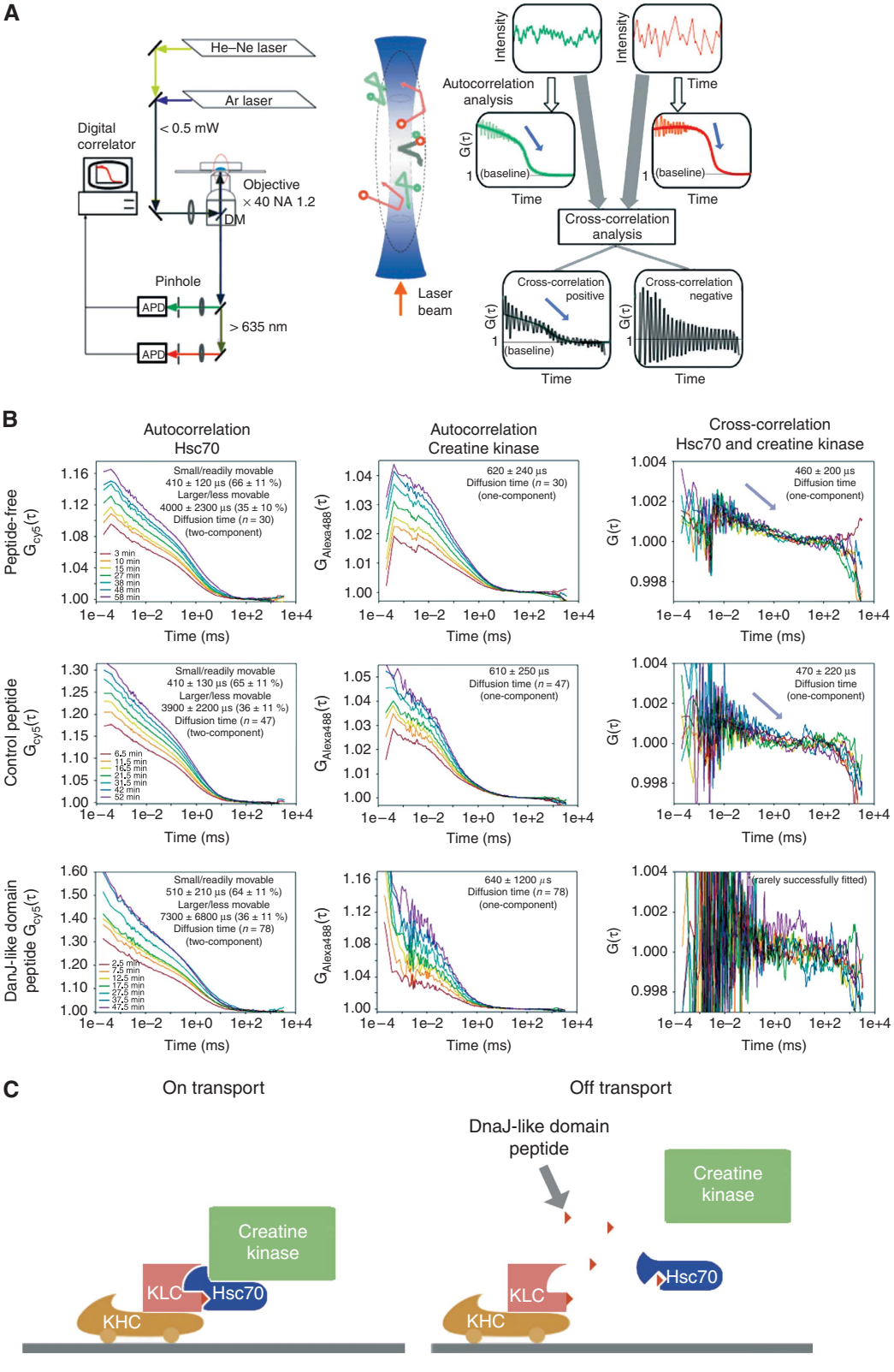

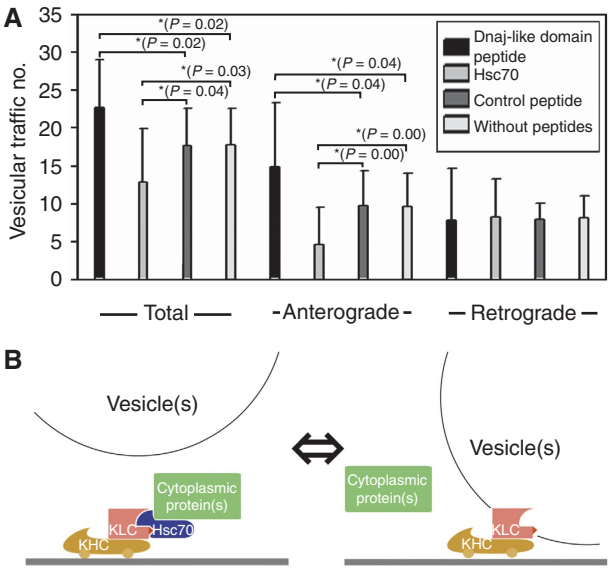

Figure 4 DnaJ-like domain peptide treatment and vesicular transport in squid giant axons. (**A**) The number of vesicles passing across the fixed line with a unit length (10 μm) for 1 min, both antero- and retrogradely in VEC-DIC images. (Left) Total vesicular traffic (both antero- and retrograde transport) was promoted by DnaJ-like domain peptide application, and inhibited by Hsc70 treatment, when compared with control peptide applied or untreated specimen. (Middle) Anterograde vesicular traffic was increased in the presence of DnaJ-like domain peptide, and inhibited by Hsc70 in the same way as the cases shown in the left column. (Right) Retrograde vesicular traffic was not affected by peptide or Hsc70 treatments. Bars indicate standard deviations. Pairs with asterisk indicate their *P*-values are <0.05 (Mann–Whitney tests, $n=16$ for each). (**B**) DnaJ-like domain of KLC serves to anchor KLC to Hsc70. (Left) Slow axonal transport mode. By associating with DnaJ-like domain in the TPR of KLC, activated Hsc70 binds to cytoplasmic proteins. (Right) Fast axonal transport mode. The same domain binds to a membranous vesicle.

domain peptide diminishes cross-correlation signal, reflecting the loss of the interaction between Hsc70 and creatine kinase (Figure 3C).

DnaJ-like domain peptide reinforces, but Hsc70 blocks membranous organelle transport

A preceding report indicating deprivation of Kinesin-1 from membranous vesicle by Hsc70, and inhibitory function of KLC on this reaction (Tsai *et al*, 2000), showed that Hsc70 inhibits fast axonal transport, whereas our experimental results (Figure 3C) suggests that Hsc70 support slow axonal transport. To evaluate the relevance of DnaJ-like domain of KLC and Hsc70 on fast axonal transport, we observed fast vesicular traffic in extruded squid giant axons, using video-enhanced contrast/differential interference-contrast (VEC-DIC) microscopy (Brady *et al*, 1993; Takeda *et al*, 2000). Surprisingly, the treatment for inhibiting the interaction between Hsc70 and Kinesin-1 motor complex by DnaJ-like domain peptide induced promoted fast transport. We counted the number of vesicles passing across the fixed line with a unit length (10 μm) for 1 min, both antero- and retrogradely in VEC-DIC images (Figure 4A) (Takeda *et al*, 2000). When we added DnaJ-like domain peptide, we observed enhanced vesicular movements, especially in anterograde direction, compared with those of the cases with control peptide or untreated axoplasm. On the other hand, when we added Hsc70, the vesicular movements were blocked, especially in anterograde direction, compared with those of the cases with control peptide or untreated axoplasm (all *P*-values with asterisk <0.05, Mann–Whitney test, $n=16$ for each.). Both DnaJ-like domain peptide and Hsc70 did not affect the vesicular transport of retrograde direction. There was no difference in vesicular movement of both directions between the samples with control peptide and untreated axoplasm. We consider the concentrations of DnaJ-like domain peptide and Hsc70 introduced here is well controlled within the effective dose range. To monitor the diffusion of Hsc70 into the axoplasm, Cy5-labelled Hsc70 was applied to the axoplasm to inhibit organelle movement. Fluorescent Hsc70 was found to penetrate the axoplasm with a time course similar to that found for the appearance of the inhibitory effect (data not shown). The effect by Hsc70 was first detected within 5 min after protein addition and became apparent throughout the axoplasm by 30 min. The effects by peptide addition were apparent within a minute after peptide addition, and detected throughout the axoplasm by 5 min, reflecting the faster penetration of peptide than Hsc70. The image by VEC-DIC microscopy was collected from the axoplasm near (about 50 μm) the external surface. (Examples of both DnaJ-like domain peptide and Hsc70 effects on fast vesicular traffic in extruded squid giant axons are shown in Supplementary Figure S1 and Supplementary Videos.) These findings support the hypothesis that DnaJ-like domain of KLC might have a 'molecular switchover' function by Hsc70 in the determination of molecular motor Kinesin-1 usage in fast or slow axonal transport (Figure 4B).

Generation of transgenic mice with impaired formation of the transporting complex

On the basis of the observations from the squid experiments, we decided to generate transgenic mice with impaired formation of the transporting complex for slow axonal transport by using the DnaJ-like domain of KLC. We constructed vector (Thy1-deleted KLC-IRES-GFP) to overexpress KLC that lacked the DnaJ-like domain and intended to generate the dominant-negative condition on slow axonal transport (Figure 5A). Among several lines, we decided to use lines (m3m4 and m3m5), in which the transgene was expressed moderately in retinal ganglion cells. At first sight, the transgenic mice appeared to behave normally, and lived out the natural life span of their wild-type littermates.

Impaired slow axonal transport and accelerated fast axonal transport in optic nerve axons in transgenic mice

To check the dominant-negative effect of KLC that lacked the DnaJ-like domain on slow axonal transport *in vivo*, we performed metabolic-labelling studies by ^{35}S methionine injection into the vitreous bodies of transgenic mice eyeballs. We used young transgenic mice (younger than 4 months old) to check the primary effect of transgene before other pathological or behavioural phenotype appeared. After 2, 10 or 15 days, consecutive serial segments (1 mm in length) of the optic nerves were processed by centrifugation and separated by one-dimensional electrophoresis. The gels were then exposed to imaging plates, and the profiles of specific bands were analysed (Figure 5B). Our preliminary experiment of two-dimensional electrophoresis using extracts from

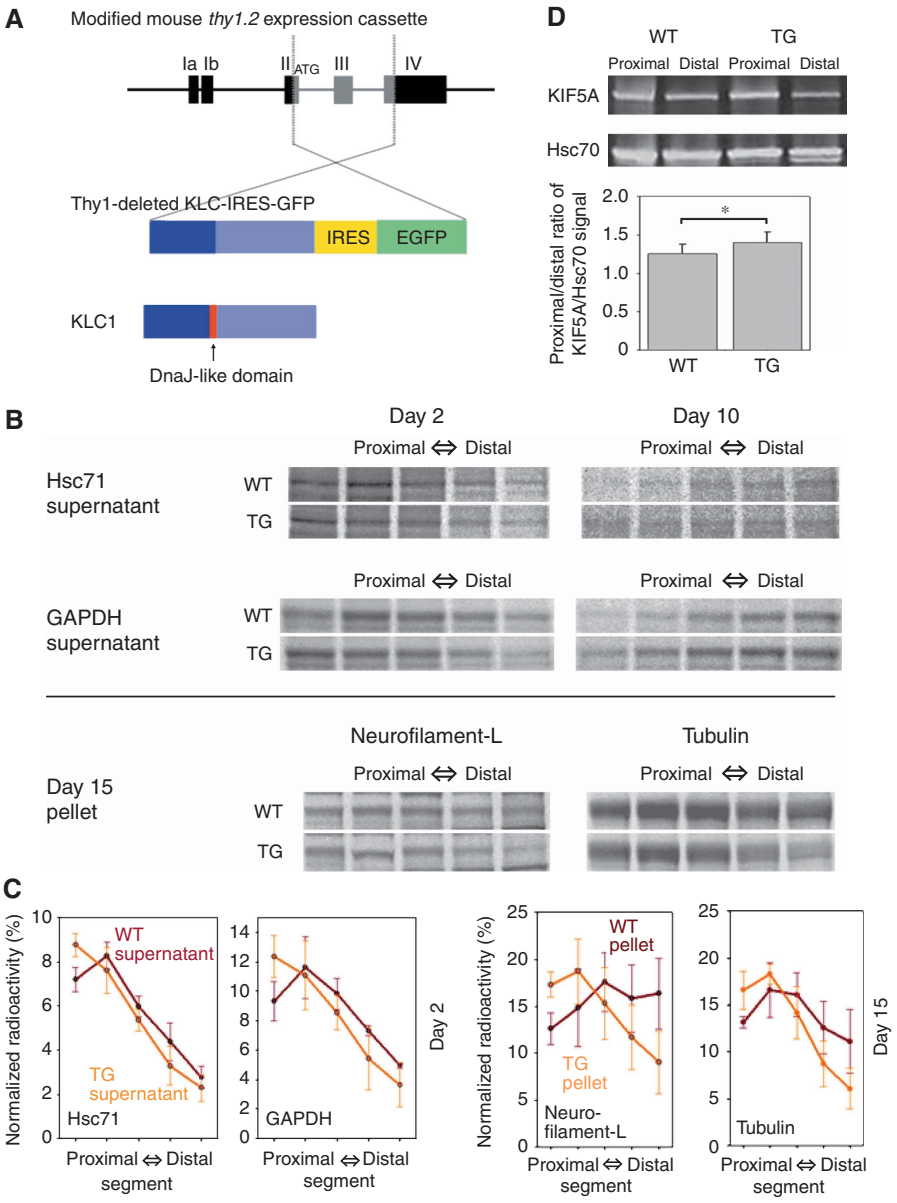

Figure 5 Transgenic mice generation and axonal transport analysis in their optic nerve axons. (**A**) Vector construction for the transgenic mice. Thy1-deleted KLC-IRES-GFP expresses KLC in which the DnaJ-like domain is deleted and GFP bicistronically under the control of the *thy1.2* promoter. (**B**) Slow axonal transport profile analysed by metabolic-labelling studies. We injected ^{35}S methionine into the vitreous bodies of mouse eyeballs. After 2, 10 or 15 days, consecutive serial segments of the optic nerves were processed. WT (upper panels) and TG (lower panels) show the results for the wild-type and transgenic mice, respectively. The results of supernatants of Hsc71 and GAPDH at day 2/10 and pellets of neurofilament (L; low-molecular weight) and tubulin at day 15 are shown. (**C**) Profiles of specific bands based on the results shown in (**B**). Bars show the standard deviation. (**D**) Fast axonal transport analysed by sciatic nerve ligation studies. We ligated sciatic nerves, and 6 h later, collected nerve segments (3 mm) proximal and distal to the ligature. Sciatic nerve segments were analysed by western blot. WT (left panels) and TG (right panels) show the results for the wild-type and transgenic mice, respectively. The proximal/distal ratios of KIF5A (fast axonal marker)/Hsc70 (internal control) signal were 1.254 ± 0.123 ($n = 8$) for wild-type mice and 1.404 ± 0.135 ($n = 8$) for transgenic mice.

the metabolically labelled optic nerve axons revealed that some of the radioactive spots have unique molecular weight values. Some of these spots were Hsc71-, glyceraldehyde-3-phosphate dehydrogenase (GAPDH)-, neurofilament protein (low-molecular weight)- and tubulin-origin (S Terada, unpublished data, 2009).

We compared the radioactivity profiles of these proteins, and found that the movement of the profile peak was retarded in transgenic mice. At day 2, the profile peaks of supernatants containing Hsc71 (product of the mouse HSP70 multigene family) and GAPDH were located in the second proximal segment in wild-type mice, whereas they remained in the most proximal segment in the transgenic mice. This retardation in transgenic mice continued later at day 10. At day 15, the gravity centres of the profiles from pellets of neurofilament protein (low-molecular weight) and tubulin were less advanced in the transgenic mice (Figure 5B). Normalized radioactivity curves were different between transgenic and wild-type mice (at day 2, *P*-value of Hsc71 $0.020 < 0.05$, GAPDH $0.019 < 0.05$; at day 15, neurofilament protein $0.000 < 0.01$, tubulin $0.005 < 0.01$, two-way repeated-measures analysis of variance, $n = 3$ for each genotypes).

These results showed that both slow components a (SCa, cytoskeletal proteins) and b (SCb, other cytoplasmic proteins) were impaired (Figure 5C).

Next, we explored the fast axonal transport in our mice by sciatic nerve ligation studies. We ligated sciatic nerves, and 6 h later, collected nerve segments (3 mm) proximal and distal to the ligature. Sciatic nerve segments were homogenized, centrifuged, and analysed by western blot. We used KIF5A, a neuron-specific isoform of Kinesin-1, as a fast axonal transport marker (Zhao *et al*, 2001). Our preliminary experiment demonstrated that the contrast and density of the band by KIF5A on western blot is more than those of the other markers, APP and KIF1A for example, and we can measure its density more exactly than others. The accumulating time course of KIF5A was indistinguishable from other markers. To correct the possible sample volume variation, we used Hsc70 signal as internal control. As the ligation time is sufficiently short for slow axonal transport, the band density of a specific cytosolic protein, such as Hsc70 or creatine kinase, in segments of both transgenic and wild-type animals does not alter during ligation and could serve practically as an internal control for normalizing the quantity of the samples. The proximal/distal ratios of KIF5A/Hsc70 signal were 1.254 ± 0.123 ($n = 8$) for wild-type mice and 1.404 ± 0.135 ($n = 8$) for transgenic mice. The accumulation of KIF5A signal was more prominent in the transgenic mice than wild-type animals ($P = 0.046 < 0.05$, Mann–Witney test; Figure 5D), suggesting the moderately accelerated fast axonal transport in our transgenic mice.

Optic nerve axonopathy without elevation of intraocular pressure in transgenic mice

To examine what kind of impediment the transgenic mice suffered from, we checked any pathological changes in the optic nerve at 2 years of age. Though young transgenic mice (younger than 4 months old) had no apparent pathological or behavioural phenotype, semi-thin sections of the transgenic mice at 2 years of age stained with toluidine blue showed degenerating axons as accumulating darkly stained structures, and patches of empty space without axons in the peripheral areas (Figure 6A, black and red circles). We counted the number of axons with accumulating darkly stained structures and axon-free patches that cannot be covered within circles of 5 μm in diameter, and found more in transgenic than wild-type animals (darkly stained structure, transgenic mice 341.7 ± 19.6, wild-type animals 203.0 ± 21.1, *P*-value $0.00 < 0.05$, Mann–Whitney test, $n = 3$ for each: axon-free patch, transgenic mice 142.3 ± 9.6, wild-type animals 68.0 ± 13.0, *P*-value $0.00 < 0.05$, Mann–Whitney test, $n = 3$ for each.). In some cases, we could find abnormally giant swollen axon fibres that we never encounter in optic nerves of wild-type littermates (Figure 6A, asterisks). We counted the frequency of large swollen axons with > 10 μm-major diameter, and those axons are found only in transgenic mice (transgenic mice 3.7 ± 0.6, wild-type mice 0.0 ± 0.0, *P*-value $0.00 < 0.05$, Mann–Whitney test, $n = 3$ for each.). These pathological features resemble and are reminiscent of changes in earlier reported glaucoma model (Senatorov *et al*, 2006).

Successive ultrastructural studies showed that the axonal cytoarchitecture was frequently altered. We found that some of the axons, especially those with 0.6–0.9 μm in diameter, seemed to be reduced, whereas those with 0.9–2 μm in diameter increased, compared with those of wild-type mice, suggesting the slight dilation in diameter. The total quantification data on the axon-diameter difference between transgenic and wild-type mice are shown in the diameter distribution curve shown in Supplementary Figure S2. The percentage of axons with 0.6–0.9 and 0.9–2 μm in diameter is 25.8 and 16.2 in a wild-type mouse, 22.4 and 23.5 in a transgenic mouse, respectively, and in both axon groups, the values are different between genotypes ($P = 0.000 < 0.001$, χ^2 test). Cross-sections of those presumably dilated axons often showed a biased distribution of microtubules in the axoplasm (Figure 6B). In such axons, the cytoarchitecture was less organized, and cytoskeletal structures such as neurofilaments and cytoskeleton-associated structures appeared to be twisted and sparse.

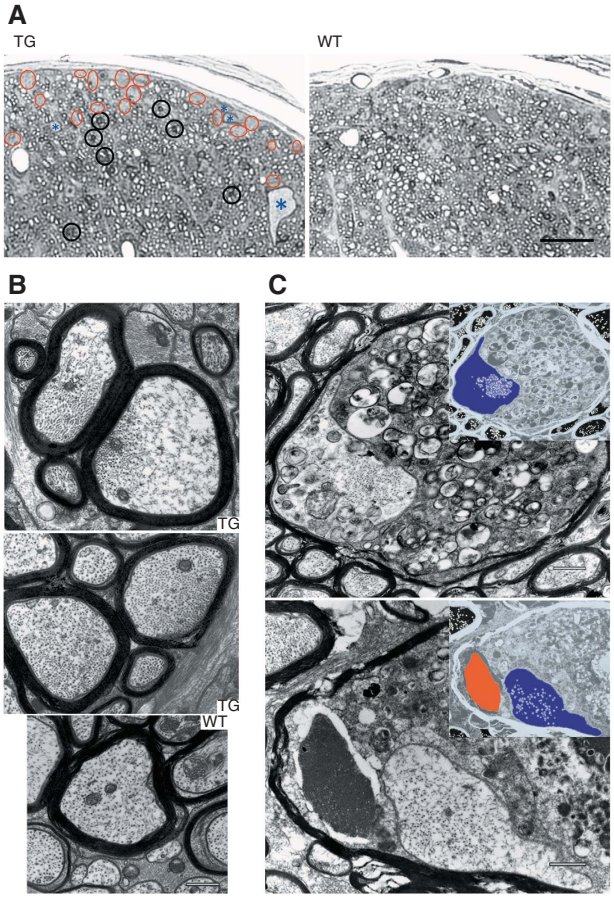

Figure 6 Deteriorated axonal cytoarchitecture and 'dying-back' oligodendrogliopathy with late-onset axonal degeneration in transgenic mice. (**A**) Semi-thin sections of the transgenic mice stained with toluidine blue. Degenerating axons as accumulating darkly stained structures (black circles) and patches of empty space without axons in the peripheral areas (red circles) are prominent in transgenic mice (TG). Abnormally giant swollen axons (asterisks) that we never encounter in wild-type littermate (WT) are conspicuous in the dorsal compartment of optic nerves. Bar: 20 μm. (**B**) The slightly dilated axons in transgenic mice (TG) show a biased distribution of microtubules in the axoplasm, compared with wild-type mice (WT). Bar: 500 nm. (**C**) 'Dying-back' oligodendrogliopathy of optic nerves, showing atrophic axoplasm (depicted in blue in the negatives), and the severely degenerated and swollen periaxoplasmic inner loop of oligodendroglia. In the lower panel, note the crystalline inclusions within the degenerating inner loop (depicted in red in the negative) of oligodendroglia. Bars: 500 nm.

We performed morphometric analysis on the appearance rate of this biased distribution of microtubules in the axoplasm such as that shown in Figure 6B. We divided the cross-sections of optic nerves into four compartments (dorsolateral, dorsomedial, ventrolateral and ventromedial) and determined the position of gravity centre in each compartment. We took electron micrographs within 25 μm from these gravity centres, and counted the number of axons with disorganized structures. As biased distributions of microtubules are more apparent and easy to observe in large-diameter axons, we selected axons with >0.7 μm-minor diameters. In a transgenic mouse, 543 axons out of 904 had a biased distribution of microtubules, whereas 12 axons out of 860 in a wild-type animal. Thus, axons with biased microtubule distribution such as shown in Figure 5B were found more frequently in transgenic mice axons compared with wild-type animals ($P=0.000<0.001$, χ^2 test).

We also observed large swollen fibres with atrophic axoplasm, and in these axons, the periaxoplasmic inner loop of the oligodendroglia projection, surrounding the atrophic axoplasm, was severely degenerated (Figure 6C). These pathological changes could be described as slowly progressive optic nerve axonopathy and 'dying-back' oligodendrogliopathy. In some cases, we found crystalline inclusions within the degenerating inner loop of oligodendroglia (Figure 6C, lower panel). The term 'dying-back' used here refers to gliopathological change that has a distal to proximal gradient of pathology along the long cellular projection of oligodendroglia, which forms myelin sheath (Lassmann *et al*, 1997). We observed the same kind of pathological changes ('dying-back' myelinopathy) as well as motor and sensory axonopathy of sciatic nerves in other transgenic mice lines, expressing the same construct in the peripheral nervous system. (See Supplementary data; Supplementary Figure S3 online for detail.) As the transgene expression is driven by neuron-specific *thy1.2* promoter, these features represent the axonal damage triggering demyelination, that is inside-out consequences of degeneration, from the axon to the inner loop of myelin, and then to the myelin sheath (Tsunoda and Fujinami, 2002).

Next we found that thinner axon group decrease was prominent and that the appearance of above-mentioned abnormally dilated axons was characteristic in the transgenic mice. We divided the cross-sectional area of optic nerves into four compartments, dorsomedial, dorsolateral, ventromedial and ventrolateral, and counted the number of thin axons (diameter <2 μm) of each division. The mean number of wild-type mice was 397.5 ± 147.2 ($n=4$), whereas that of the transgenic mice was 54.8 ± 27.2 ($n=4$), and the decrease of thinner axons was apparent ($P=0.017<0.05$, Student's *t*-test). Abnormally giant swollen axons seemed only in the dorsal compartment. These changes indicated that the slow axonal transport blockage might induce slowly progressive axonopathy in the optic nerves. Another morphometric analysis of the samples whose abnormally giant swollen axons were less apparent is shown in Supplementary Figure S2. The pathological change is more dominant in the dorsal compartment.

As it is known that high intraocular pressure (IOP) induces glaucomatous optic neuropathy, we measured the IOP in 21- and 22-month-old mice (Aihara *et al*, 2002). Although the mean IOP of wild-type mice was 14.09 ± 0.43 mm Hg ($n=4$), that of the transgenic mice was 13.78 ± 0.30 mm Hg ($n=4$), and there was no apparent difference between the genotypes ($P=0.30$, Student's *t*-test). Thus, our mice showed primary optic neuropathy without elevation of IOP.

Discussion

Slow axonal transport of general cytoplasmic proteins are dependent on Hsc70, scaffolding between KLC and cytoplasmic protein cargos

The molecular motor for slow transport is assumed to be Kinesin-1 (Brown, 2003; Terada, 2003), that is the same motor for fast transport with a large difference in duty cycle, but how it can interact with cargo proteins has been an open question. Our studies have revealed that Hsc70 is well suited for intercalating motor–cargo interactions through the TPR region of KLC. The high conservation of TPR regions in both orthologues and paralogues suggests an essential function (McCart *et al*, 2003). A function in cargo binding has been inferred from observations that (1) an antibody against this region can induce vesicle release from kinesin (Stenoien and Brady, 1997) and (2) members of the JIP family of scaffolding proteins bind to this region (Bowman *et al*, 2000; Verhey *et al*, 2001). However, as the TPR region can interact with various kinds of partner (Lamb *et al*, 1995; Blatch and Lassle, 1999; D'Andrea and Regan, 2003), we need to examine its direct interactions *in situ*. To examine the scaffolding function of Hsc70 between KLC and cytoplasmic protein cargos *in vivo*, we monitored the movement and complex formation of Hsc70 and cytoplasmic proteins using CLSM and FCCS. We could detect the cross-correlation signal between Hsc70 and creatine kinase in live squid axoplasm. The peptide fragment of the DnaJ-like domain of KLC disrupted cytoplasmic protein transport by disrupting the motor–cargo interaction (Figure 3C). By associating with DnaJ-like domain proteins including KLC, the ADP form of Hsc70 binds to cytoplasmic proteins, and the injected DnaJ-like domain peptide competes this association, thus disrupting the interaction between KLC and Hsc70. As the peptide binding is weak and the squid giant axoplasm is ATP-rich, dissociated ADP-form Hsc70 is converted into the ATP form, thus releasing its substrates, including creatine kinase. Biochemical immunoprecipitation data on the complex of KLC/Hsc70/creatine kinase and *in vitro* FCCS measurements using Hsc70 and creatine kinase supported this mechanism, as DnaJ-like domain peptide effect of creatine kinase dissociation from the complex was dependent on ATP and the cross-correlation signal increased with ATP consumption over time, and the DnaJ-like domain peptide inhibited this reaction (data not shown).

As far as we are concerned, we consider general cytoplasmic proteins that can bind to Hsc70 could be transported by this mechanism. The exceptions are some of the cytoskeletal proteins such as tubulin or actin. They do not bind to Hsc70, and our preliminary results indicate that DnaJ-like domain peptide has less effect on tubulin transport than other general cytoplasmic proteins (data not shown).

Hsc70 might switch Kinesin-1 between fast and slow axonal transport in a DnaJ-like domain of KLC-dependent manner

A preceding report indicating deprivation of Kinesin-1 from membranous vesicle by Hsc70, and inhibitory function of

KLC on this reaction (Tsai *et al*, 2000), showed that Hsc70 inhibits fast axonal transport, whereas our experimental result suggests that Hsc70 support slow axonal transport. Surprisingly, the treatment for inhibiting the interaction between Hsc70 and Kinesin-1 motor complex induced both deteriorated slow transport and promoted fast transport. From these consequences, we postulated that the DnaJ-like domain of KLC serves to anchor KLC to Hsc70, and that Hsc70 might be a molecular change-over switch for slow and fast axonal transport. This hypothesis is based on the fact that putative Hsc70-binding domain within KLC, that is DnaJ-binding domain, almost correspond to the TPR domain, which binds to membranous organelles. This suggests that Hsc70 and membranous organelles bindings to KLC are mutually exclusive. As slow axonal transport is dependent on Hsc70 binding to KLC, slow and fast axonal transport events might be mutually exclusive.

The system using acute preparation of squid giant axons cannot escape from the stress response induced by the experimental intervention, because longer experiments >2 h are challenges. Although the effects of Hsc70 on transport were indistinguishable within this experimental time-window, it is possible that Hsc70 might affect the transport indirectly through a stress response, possibly through the CHIP pathway. Accumulating the knowledge of the regulatory mechanism linking the motor complex with different cargos, cytoplasmic proteins or membranous organelles is indispensable to explain the whole figure of intracellular transport.

Slow axonal transport impairment and late-onset axonal degeneration

The slow axonal transport system carries various proteins to support local cellular functions. Although many studies have implied a close relationship between slow transport collapse and nerve degeneration such as glaucoma, it was difficult to identify the causal relationship from the phenomena. Our results indicate that primary slow transport perturbation might induce late-onset axonal atrophy and degeneration, along with 'dying-back' oligodendrogliopathy. These observations indicate that the primary blockage of slow transport could be the basis of neuronal degenerating processes. Strictly speaking, as our experimental result indicates that both slow and fast axonal transport systems are inter-dependent, analysing the two separately is impossible. Though the late-onset time course of the pathological change indicates that it might be more plausible to interpret the findings based on slow axonal transport mechanism, the possibility remains that the effects are the sum of consequences and that impaired transport might arise from a dysregulation of pathways away from the mechanism we have postulated.

We have identified adult-onset axonal changes that are most pronounced in optic nerve areas known to be particularly vulnerable to glaucomatous pathogenesis. In 21- or 22-month-old affected mice, there was a marked reduction in the number of nerve fibres, especially in the dorsal portion, in which rodent animal models with high IOP show the most marked glaucomatous changes (Morrison *et al*, 1997; Mabuchi *et al*, 2003), although the IOP was within the normal range in our mice. Interestingly, many of the remaining fibres had large diameters, reminiscent of glaucoma animal models such as DBA/2J mice (John *et al*, 1998). Our findings and a recent report describing the neuroprotective effect of Hsp70 in a rat ocular hypertension model (Ishii *et al*, 2003) collectively suggest that slow axonal transport blockage could trigger the glaucomatous optic neuropathy.

Finally, it has not escaped our notice that the chaperone-assisted mechanism of slow axonal transport suggests a promising basis for gene therapy for neuronal degenerating diseases, using molecular chaperones or motor complexes as tools. In fact, overexpression of Hsp70 has been reported to rescue neuronal degeneration in some animal models (Cummings *et al*, 2001; Auluck *et al*, 2002; Adachi *et al*, 2003; Jin *et al*, 2003), and further elucidation of the molecular network of chaperones and molecular motors will unravel the mysteries of various neuronal degenerating diseases.

Materials and methods

Immunoprecipitation

Mouse sciatic nerves were dissected and homogenized in ice-cold homogenizing buffer (50 mM phosphate buffer, 150 mM NaCl, 1% deoxycholate, 1% Triton X-100, 0.5% SDS, 1 mM orthovanadate, supplemented with proteinase inhibitors) then centrifuged for 20 min at 17 000 *g*. Immunobeads and control beads were prepared using anti-KLC1 (H-75, Santa Cruz Biotechnology, CA), anti-Hsc70 (SPA-815, Stressgen, BC, Canada) or anti-creatine kinase (N-20, Santa Cruz Biotechnology, CA) antibodies, and the supernatants were incubated overnight at 4°C (Johanson *et al*, 1995). During incubation, synthetic peptides (5 mM of DLEKTSGHDHPDVATMLN (DnaJ-like domain) or NLMTAVDPHDHGSTKELD (reversed DnaJ-like domain)), ATP (2 mM) or apyrase (10 U/ml) were added, if necessary. The precipitates were then washed and analysed by western blot.

Reagents for transport analysis using squid giant axons and injection procedures

Creatine kinase (Roche Diagnostics, Mannheim, Germany) and recombinant mouse Hsc70 (BioDynamics Laboratory, Tokyo, Japan) were labelled with Alexa 488 succinate dye (Molecular Probes, OR) and Cy-5 succinate dye (Amersham Biosciences, NJ), respectively. Fab fragment of anti-Kinesin-1 monoclonal antibody (H2) (Chemicon, Temecula, CA) and normal mouse IgG_{2b} (Zymed, San Francisco, CA) were prepared by ImmunoPure Fab kit (Pierce, Rockford, IL) and used, as described earlier (Terada *et al*, 2000). To deplete Fab fragment of H2, we used recombinant Kinesin-1 beads (the N-terminal 411 amino acids of KIF5C with histidine-tag bound with metal chelating resin (Talon, Clontech, Palo Alto, CA)), also as described earlier (Terada *et al*, 2000). Synthetic peptides for injection (DnaJ-like domain, reversed DnaJ-like domain, reversed sequences of the carboxy terminal of Hsc70 #1 (DVEEITPGSGSG), reversed sequences of the carboxy terminal of Hsc70 #2 (DVEEVTPGSYGG)) were purchased from Research Genetics (AL). Squid giant axon preparation and protein injection were performed as described earlier (Terada *et al*, 2000).

Observation of injected fluorescent proteins by CLSM

We estimated the speeds of injected fluorescent proteins on transport at RT (20–24°C) as described earlier (Terada *et al*, 1996, 2000) using a CLSM unit (μRadiance MR/AG-2; Nippon Bio-Rad Laboratories, Tokyo, Japan) attached to a fixed-stage upright fluorescent microscope (BX50WI-FL/DIC; Olympus, Tokyo, Japan).

FCCS measurements and analysis

FCCS measurements were carried out at RT (20–24°C) using a ConfoCor2 (Carl Zeiss, Jena, Germany), which consisted of a CW argon laser, a helium–neon laser, a water-immersion objective lens (C-Apochromat, ×40, 1.2 N.A.) and two channels of avalanche photodiodes (SPCM-200-PQ; EG & G Optoelectronics, Quebec, Canada). The fluorescence autocorrelation functions of the red and green channels and the fluorescence cross-correlation function were calculated, fitted by a one- or two-component model, and then, the average numbers of red fluorescent particles, green fluorescent particles and particles that have both red and green fluorescence were calculated, as described earlier (Saito *et al*, 2004).

Observation by VEC-DIC microscopy

An Eclipse TE2000-U microscope equipped with VEC–DIC gadgetry (Nikon, Tokyo, Japan) was used for observing the vesicle traffic within extruded squid axoplasm at RT (20–24°C) (Brady *et al*, 1993; Takeda *et al*, 2000). We used a $\times 60$, 1.4 N.A. plan-apochromat objective and a 1.4 N.A. condenser. The DIC image was projected to a video camera (ORCA-ER, Hamamatsu Photonics, Hamamatsu, Japan). With accompanying software Aquacosmos, the image of moving organelles was contrast enhanced. DnaJ-like domain peptide or Hsc70 were applied to the bath solution (Terada *et al*, 2000). Vesicular structures moving both antero- and retrogradely were captured in the same video frames. The volume of organelle traffic was estimated by the number of vesicles passing across the fixed line with a unit length (10 μm) per 1 min (Takeda *et al*, 2000).

Generation of transgenic mice

We generated transgenic founders with elements from the murine *thy1.2* vector (Andra *et al*, 1996; Caroni, 1997; Feng *et al*, 2000), and deleted mouse *Kinesin light chain 1* (*Klc1*) (deleted +718 to +771) plus IRES-EGFP from the pIRES2-EGFP vector (BD Biosciences Clontech, CA). Transgenic mice (TgN(Thy1-deleted KLC-IRES-GFP)m3m4Noh and TgN(Thy1-deleted KLC-IRES-GFP)m3m5Noh) were generated by injecting gel-purified DNA into fertilized oocytes using standard techniques (Hogan *et al*, 1994).

Metabolic-labelling studies

Metabolic-labelling studies using optic nerve axons were performed, as described earlier (Elluru *et al*, 1995). In brief, retinal ganglion cells from transgenic mice were radiolabelled *in situ* with 3×10^6 becquerels (80 μCi) of ^{35}S-methionine (Amersham Biosciences, NJ) by intravitreal injection. After the injection, the mice were killed and their optic pathways were cut into five consecutive segments of 1.0 mm in length. Each segment was homogenized, centrifuged and the Triton-insoluble cytoskeleton and soluble protein fractions were analysed in polyacrylamide gels, and quantified using imaging plates (BAS-2000; Fuji Photo Film, Tokyo, Japan).

Sciatic nerve ligation studies

Mice were anesthetized, and their skin on the lateral surface of the thigh was incised. The sciatic nerve was exposed and ligated using 6-0 nylon sutures. Six hours later, nerve segments (3 mm) proximal and distal to the ligature were collected and frozen in liquid nitrogen. Sciatic nerve segments were homogenized, centrifuged and the pellet fractions were analysed by western blot. The antibodies used were anti-KIF5A rabbit polyclonal antibody (Zhao *et al*, 2001) and anti-Hsc70 rat monoclonal antibody (SPA-815). The accumulation rate of KIF5A signal at proximal side (proximal side/distal side), standardized by those of Hsc70 signal, was measured by Image J (Rasband, WS, ImageJ, US National Institutes of Health, Bethesda, Maryland, http://rsb.info.nih.gov/ij/, 1997–2008).

Morphological studies of optic nerve axons

Samples for morphological studies were prepared as described earlier (Terada *et al*, 1996, 2000). For electron microscopy, the ultrathin sections were examined under a transmission electron microscope (1200EX; JEOL, Tokyo, Japan) at an accelerating voltage of 80 kV. For light microscopy, the sections were stained with toluidine blue and photographed. We counted the number of axons with accumulating darkly stained structures and axon-free patches that cannot be covered within circles of 5 μm in diameter. We also counted the number of thin axons (diameter <2 μm). Morphometric analysis on the appearance rate of the biased distribution of microtubules in the axoplasm was performed by examining the axons (with >0.7 μm-minor diameter) located within 25 μm from putative gravity centres of four compartments (dorsolateral, dorsomedial, ventrolateral and ventromedial) of optic nerve cross-section (see Supplementary data for detail).

IOP measurement

IOP measurement was performed as described earlier (Aihara *et al*, 2002).

All of the animal experiments were carried out under the control of the Guideline for Animal Experimentation in Tokyo University and the protocol was approved by the Animal Care and Use Committee of Tokyo University Graduate School of Medicine.

Supplementary data

Supplementary data are available at *The EMBO Journal* Online (http://www.embojournal.org).

Acknowledgements

We thank Dr GC Sharp (Harvard Medical School) and Professors GS Bloom and A Periasamy (University Virginia) for their comments on our manuscript. We thank Professors H Okazawa and H Mizusawa (Tokyo Medical and Dental University) for their inspection and comments on our neuropathological findings, all the members of the Hirokawa and the Terada laboratories for their help, especially S Takeda (now in Yamanashi University) for his assistance with the metabolic-labelling studies, Y Kinoshita (now in Nagoya City University) for his *klc1* cDNA clone and M Taguchi (in the Terada laboratory) for her assistance in data collection. The authors also thank JR Sanes (Harvard University) for the *thy1.2* vector. This work was supported by a PRESTO program grant from Japan Science and Technology Agency (JST) and by the 21st COE (Centre of Excellence) program from Japan Society for the Promotion of Science (JSPS) to ST, by a Grant-in-Aid for Specially Promoted Research from the Japan Ministry of Education, Culture, Sports, Science and Technology (MEXT) and the Global COE program from JSPS to NH. ST conceived, carried out the experiments, and wrote the paper; MK assisted the FCCS measurement; MA carried out the IOP measurement; ST generated the transgenic mice under supervision of YT and NH supervised the project and edited the paper. All the authors discussed the results.

Conflict of interest

The authors declare that they have no conflict of interest.

References

Adachi H, Katsuno M, Minamiyama M, Sang C, Pagoulatos G, Angelidis C, Kusakabe M, Yoshiki A, Kobayashi Y, Doyu M, Sobue G (2003) Heat shock protein 70 chaperone overexpression ameliorates phenotypes of the spinal and bulbar muscular atrophy transgenic mouse model by reducing nuclear-localized mutant androgen receptor protein. *J Neurosci* **23:** 2203–2211

Aihara M, Lindsey JD, Weinreb RN (2002) Reduction of intraocular pressure in mouse eyes treated with latanoprost. *Invest Ophthalmol Vis Sci* **43:** 146–150

Andra K, Abramowski D, Duke M, Probst A, Wiederhold KH, Burki K, Goedert M, Sommer B, Staufenbiel M (1996) Expression of APP in transgenic mice: a comparison of neuron-specific promoters. *Neurobiol Aging* **17:** 183–190

Auluck PK, Chan HY, Trojanowski JQ, Lee VM, Bonini NM (2002) Chaperone suppression of alpha-synuclein toxicity in a Drosophila model for Parkinson's disease. *Science* **295:** 865–868

Baas PW, Brown A (1997) Slow axonal transport: the polymer transport model. *Trends Cell Biol* **7:** 380–384

Benaroudj N, Batelier G, Triniolles F, Ladjimi MM (1995) Self-association of the molecular chaperone HSC70. *Biochemistry* **34:** 15282–15290

Blatch GL, Lassle M (1999) The tetratricopeptide repeat: a structural motif mediating protein-protein interactions. *Bioessays* **21:** 932–939

Bourke GJ, El Alami W, Wilson SJ, Yuan A, Roobol A, Carden MJ (2002) Slow axonal transport of the cytosolic chaperonin CCT with Hsc73 and actin in motor neurons. *J Neurosci Res* **68:** 29–35

Bowman AB, Kamal A, Ritchings BW, Philp AV, McGrail M, Gindhart JG, Goldstein LS (2000) Kinesin-dependent axonal transport is mediated by the sunday driver (SYD) protein. *Cell* **103:** 583–594

Brady ST, Lasek RJ (1981) Nerve-specific enolase and creatine phosphokinase in axonal transport: soluble proteins and the axoplasmic matrix. *Cell* **23:** 515–523

Brady ST, Richards BW, Leopold PL (1993) Assay of vesicle motility in squid axoplasm. *Meth Cell Biol* **39:** 191–202

Brown A (2003) Axonal transport of membranous and nonmembranous cargoes: a unified perspective. *J Cell Biol* **160:** 817–821

Caroni P (1997) Overexpression of growth-associated proteins in the neurons of adult transgenic mice. *J Neurosci Methods* **71:** 3–9

Cummings CJ, Sun Y, Opal P, Antalffy B, Mestril R, Orr HT, Dillmann WH, Zoghbi HY (2001) Over-expression of inducible HSP70 chaperone suppresses neuropathology and improves motor function in SCA1 mice. *Hum Mol Genet* **10:** 1511–1518

D'Andrea LD, Regan L (2003) TPR proteins: the versatile helix. *Trends Biochem Sci* **28:** 655–662

de Waegh S, Brady ST (1989) Axonal transport of a clathrin uncoating ATPase (HSC70): a role for HSC70 in the modulation of coated vesicle assembly *in vivo*. *J Neurosci Res* **23:** 433–440

Elluru RG, Bloom GS, Brady ST (1995) Fast axonal transport of kinesin in the rat visual system: functionality of kinesin heavy chain isoforms. *Mol Biol Cell* **6:** 21–40

Feng G, Mellor RH, Bernstein M, Keller-Peck C, Nguyen QT, Wallace M, Nerbonne JM, Lichtman JW, Sanes JR (2000) Imaging neuronal subsets in transgenic mice expressing multiple spectral variants of GFP. *Neuron* **28:** 41–51

Galbraith JA, Gallant PE (2000) Axonal transport of tubulin and actin. *J Neurocytol* **29:** 889–911

Galbraith JA, Reese TS, Schlief ML, Gallant PE (1999) Slow transport of unpolymerized tubulin and polymerized neurofilament in the squid giant axon. *Proc Natl Acad Sci USA* **96:** 11589–11594

Grafstein B, Forman DS (1980) Intracellular transport in neurons. *Physiol Rev* **60:** 1167–1283

Hilfiker S, Benfenati F, Doussau F, Nairn AC, Czernik AJ, Augustine GJ, Greengard P (2005) Structural domains involved in the regulation of transmitter release by synapsins. *J Neurosci* **25:** 2658–2669

Hirokawa N, Noda Y (2008) Intracellular transport and kinesin superfamily proteins, KIFs: structure, function, and dynamics. *Physiol Rev* **88:** 1089–1118

Hirokawa N, Takemura R (2005) Molecular motors and mechanisms of directional transport in neurons. *Nat Rev Neurosci* **6:** 201–214

Hirokawa N, Terada S, Funakoshi T, Takeda S (1997) Slow axonal transport: the subunit transport model. *Trends Cell Biol* **7:** 384–388

Hogan B, Costantini F, Lacy E (1994) *Manipulating the Mouse Embryo. A Laboratory Manual*. New York: Cold Spring Harbor Laboratory

Ishii Y, Kwong JM, Caprioli J (2003) Retinal ganglion cell protection with geranylgeranylacetone, a heat shock protein inducer, in a rat glaucoma model. *Invest Ophthalmol Vis Sci* **44:** 1982–1992

Jin P, Zarnescu DC, Zhang F, Pearson CE, Lucchesi JC, Moses K, Warren ST (2003) RNA-mediated neurodegeneration caused by the fragile X premutation rCGG repeats in Drosophila. *Neuron* **39:** 739–747

Johanson SO, Crouch MF, Hendry IA (1995) Retrograde axonal transport of signal transduction proteins in rat sciatic nerve. *Brain Res* **690:** 55–63

John SW, Smith RS, Savinova OV, Hawes NL, Chang B, Turnbull D, Davisson M, Roderick TH, Heckenlively JR (1998) Essential iris atrophy, pigment dispersion, and glaucoma in DBA/2J mice. *Invest Ophthalmol Vis Sci* **39:** 951–962

Kim D, Lee YJ, Corry PM (1992) Constitutive HSP70: oligomerization and its dependence on ATP binding. *J Cell Physiol* **153:** 353–361

Kim SA, Schwille P (2003) Intracellular applications of fluorescence correlation spectroscopy: prospects for neuroscience. *Curr Opin Neurobiol* **13:** 583–590

Lamb JR, Tugendreich S, Hieter P (1995) Tetratrico peptide repeat interactions: to TPR or not to TPR? *Trends Biochem Sci* **20:** 257–259

Lassmann H, Bartsch U, Montag D, Schachner M (1997) Dying-back oligodendrogliopathy: a late sequel of myelin-associated glycoprotein deficiency. *Glia* **19:** 104–110

Mabuchi F, Aihara M, Mackey MR, Lindsey JD, Weinreb RN (2003) Optic nerve damage in experimental mouse ocular hypertension. *Invest Ophthalmol Vis Sci* **44:** 4321–4330

McCart AE, Mahony D, Rothnagel JA (2003) Alternatively spliced products of the human kinesin light chain 1 (KNS2) gene. *Traffic* **4:** 576–580

Moreno H, Yu E, Pigino G, Hernandez AI, Kim N, Moreira JE, Sugimori M, Llinas RR (2009) Synaptic transmission block by presynaptic injection of oligomeric amyloid beta. *Proc Natl Acad Sci USA* **106:** 5901–5906

Morrison JC, Moore CG, Deppmeier LMH, Gold BG, Meshul CK, Johnson EC (1997) A rat model of chronic pressure-induced optic nerve damage. *Exp Eye Res* **64:** 85–96

Nixon RA (1998) The slow axonal transport of cytoskeletal proteins. *Curr Opin Cell Biol* **10:** 87–92

Rigler R, Elson E (2001) *Fluorescence Correlation Spectroscopy: Theory and Applications*. Berlin, New York: Springer

Saito K, Wada I, Tamura M, Kinjo M (2004) Direct detection of caspase-3 activation in single live cells by cross-correlation analysis. *Biochem Biophys Res Commun* **324:** 849–854

Senatorov V, Malyukova I, Fariss R, Wawrousek EF, Swaminathan S, Sharan SK, Tomarev S (2006) Expression of mutated mouse myocilin induces open-angle glaucoma in transgenic mice. *J Neurosci* **26:** 11903–11914

Stenoien DL, Brady ST (1997) Immunochemical analysis of kinesin light chain function. *Mol Biol Cell* **8:** 675–689

Takeda S, Yamazaki H, Seog DH, Kanai Y, Terada S, Hirokawa N (2000) Kinesin superfamily protein 3 (KIF3) motor transports fodrin-associating vesicles important for neurite building. *J Cell Biol* **148:** 1255–1265

Terada S (2003) Where does slow axonal transport go? *Neurosci Res* **47:** 367–372

Terada S, Kinjo M, Hirokawa N (2000) Oligomeric tubulin in large transporting complex is transported via kinesin in squid giant axons. *Cell* **103:** 141–155

Terada S, Nakata T, Peterson AC, Hirokawa N (1996) Visualization of slow axonal transport *in vivo*. *Science* **273:** 784–788

Terasaki M, Schmidek A, Galbraith JA, Gallant PE, Reese TS (1995) Transport of cytoskeletal elements in the squid giant-axon. *Proc Natl Acad Sci USA* **92:** 11500–11503

Tsai MY, Morfini G, Szebenyi G, Brady ST (2000) Release of kinesin from vesicles by hsc70 and regulation of fast axonal transport. *Mol Biol Cell* **11:** 2161–2173

Tsunoda I, Fujinami RS (2002) Inside-out versus outside-in models for virus induced demyelination: axonal damage triggering demyelination. *Springer Semin Immunopathol* **24:** 105–125

Verhey KJ, Meyer D, Deehan R, Blenis J, Schnapp BJ, Rapoport TA, Margolis B (2001) Cargo of kinesin identified as JIP scaffolding proteins and associated signaling molecules. *J Cell Biol* **152:** 959–970

Zhao C, Takita J, Tanaka Y, Setou M, Nakagawa T, Takeda S, Yang HW, Terada S, Nakata T, Takei Y, Saito M, Tsuji S, Hayashi Y, Hirokawa N (2001) Charcot-Marie-Tooth disease type 2A caused by mutation in a microtubule motor KIF1Bbeta. *Cell* **105:** 587–597

